Multi-scale sensing of antibody-antigen interactions by organic transistors and single molecule force spectroscopy

Journal:	*ACS Nano*
Manuscript ID:	Draft
Manuscript Type:	Article
Date Submitted by the Author:	n/a
Complete List of Authors:	Casalini, Stefano; Università degli Studi di Modena e Reggio Emilia, Dipartimento di Scienze della Vita Dumitru, Andra; Instituto de Ciencia de Materiales de Madrid (CSIC), Leonardi, Francesca; Consiglio Nazionale delle Ricerche (CNR), Istituto per lo Studio dei Materiali Nanostrutturati (ISMN); Consiglio Nazionale delle Ricerche (CNR), Istituto per la Sintesi Organica e Fotoreattività Bortolotti, Carlo; Università degli Studi di Modena e Reggio Emilia, Dipartimento di Scienze della Vita Herruzo, Elena; Instituto de Ciencia de Materiales de Madrid (CSIC), Campana, Alessandra; Consiglio Nazionale delle Ricerche (CNR), Istituto per lo Studio dei Materiali Nanostrutturati (ISMN); "Alma Mater Studiorum"-Università di Bologna, Dipartimento di Chimica "G. Ciamician" de Oliveira, Rafael; São Paulo State University (UNESP) - Postgraduate Program in Materials Science and Technology, Cramer, Tobias; Consiglio Nazionale delle Ricerche (CNR), Istituto per lo Studio dei Materiali Nanostrutturati (ISMN); "Alma Mater Studiorum"-Università di Bologna, Dipartimento di Fisica e Astronomia Garcia, Ricardo; Instituto de Ciencia de Materiales de Madrid (CSIC), Biscarini, Fabio; Università degli Studi di Modena e Reggio Emilia, Dipartimento di Scienze della Vita

Multi-scale sensing of antibody-antigen interactions by organic transistors and single molecule force spectroscopy

Stefano Casalini [1,], Andra Dumitru[2], Francesca Leonardi[3,4], Carlo A. Bortolotti[1], Elena T. Herruzo[2], Alessandra Campana[5,3], Rafael F. de Oliveira[1,6], Tobias Cramer[3,7], Ricardo Garcia[2,*], Fabio Biscarini[1,3]*

[1] Life Sciences Department, Università di Modena e Reggio Emilia, Via Campi 183, 41125 Modena, Italy.

[2] Instituto de Ciencia de Materiales de Madrid (CSIC), 28049 Madrid, Spain.

[3] *CNR-ISMN* Consiglio Nazionale delle Ricerche, Istituto per lo Studio dei Materiali Nanostrutturati, Via Gobetti 101, 40129 Bologna, Italy,

[4] *CNR-ISOF* Consiglio Nazionale delle Ricerche, Istituto per la Sintesi Organica e Fotoreattività, Via Gobetti 101, I-40129 Bologna, Italy.

[5] "Alma Mater Studiorum"-Università di Bologna, Dipartimento di Chimica "G. Ciamician", Via Selmi 2, 40126 Bologna, Italy.

[6] São Paulo State University, Unesp, Postgraduate Program in Materials Science and Technology, 17033-360, Bauru, SP, Brazil

[7] "Alma Mater Studiorum"-Università di Bologna, Dipartimento di Fisica e Astronomia, Viale Berti Pichat 6/2, 40127, Italy.

KEYWORDS: organic field effect transistors, immunosensing, interleukin-4, force spectroscopy, atomic force microscopy, biorecognition, bioelectronics.

ABSTRACT

Antibody-antigen recognition in real label-free electronic biosensors is studied by a multi-scale approach combining measurements with an electrochemically-gated organic field-effect transistor (EGOFET) and single molecule force spectroscopy. Detection of anti-inflammatory cytokine, interleukin-4 (IL-4), down to 5 nM concentration is achieved using gate electrodes functionalized with IL-4 antibodies on different adhesion layers. Single force spectroscopy on the same electrodes reveals that (un-)binding force between IL-4 on the tip and its antibodies grafted onto the surface is distributed according to a chi-square distribution with mean force ≈100 pN and standard deviation ≈57 pN, independently on the adhesion layer used. Its positive skewness reflects the finite probability of multiple specific bonds between tip and surface. The control experiments (where specific binding is prevented either by the absence of the antibody or by a different antigen at the tip) yield significantly different distributions and absence of multiple binding events. The highest probability of specific binding (about 30%) is observed on Au electrodes functionalized with His-tagged protein G (PG), revealing that PG yields the largest areal density of oriented (thus available for recognition events) antibodies. The enhanced sensitivity observed in EGOFET functionalized with protein G lies in the strong electrostatic coupling of the highly oriented IL-4 antibodies with the charge carriers in the transistor channel.

1. INTRODUCTION

Immunosensing exploits one of nature's most optimized molecular recognition mechanisms, namely the interaction between an antigen (Ag) and its specific antibody (Ab)[1]. The large binding constant is exploited in Enzyme-Linked ImmunoSorbent Assay (ELISA) to detect the presence of biomarkers in bodily fluids whose concentration can be below picomolar level[2].

Detecting Ab-Ag interactions with a label-free sensing scheme requires the integration of bio-recognition moieties at a solid-liquid interface and their coupling with the transducer. The transduction of the molecular binding event should occur with minimum, if not any, further chemical amplification or development steps[3]. This is particularly relevant for point-of-care applications and in-field deployed sensors. Sensitivity and specificity both depend on how the bio-recognition groups are made available to the target and on the coupling between environment and transducer.

Among label-free immunosensors, mechanical and electronic transductions have been demonstrated[4–8]. In the case of an electronic sensor, several phenomena induced by the bio-recognition event might be exploited: local changes of electrostatic potential[9], density of charge carriers, conductivity[10], impedance[11], capacitance[12]. Simplicity of instruments and low cost are factors that make electronic transduction favoured for single-shot applications[13]. Device sensitivity is optimized by tuning the Debye length scale in biological fluids to the size of the specific binding pair. However the modulation of the Debye length is not always doable[14–16], especially in bodily fluids.

Mechanical sensors, such as quartz crystal microbalance (QCM)[5] and cantilevers[6], detect changes of mass, binding/unbinding forces and viscoelastic response. They are effective in those

regimes where electronic sensing does not provide enough sensitivity. However the interpretation of the device output in terms of specific molecular interactions is not usually straightforward.

Quantification, reproducibility and standardization are open issues in label-free immunosensing. They require multi-scale control from nanometer to hundreds of micrometers of the density, orientation and functionality of the recognition moieties on the sensing area of the device. Open questions, that also represent technological challenges, include: how to control the density of active Abs; what fraction of Abs gives rise to specific bio-recognition events; what is the detection limit of the device in terms of number of recognition events; how to make the device more effective, sensitive, and specific.

In this Paper, we propose a multi-scale approach, combining local and non-local techniques that serve to quantify antibody-antigen recognition events in label-free electronic biosensors. Our approach combines an electrolyte-gated organic field effect transistor (EGOFET) (Fig.1) and single molecule force spectroscopy (SFS) (Fig. 2) to assess specific recognition on device-relevant Au surfaces in the limit of strong electrostatic screening regime.

In EGOFET the gate electrode immersed in the electrolyte solution is functionalized with a bio-recognition moiety. In the presence of the target molecule in solution, a number of local binding events at the gate electrode leads to a potential change [17–19]. This change affects the electrostatic potential at the electrolyte solution/organic semiconductor interface, which couples to the semiconductor channel via the capacitance C_{DL} of the Debye-Helmholtz layer. Being C_{DL} on the order of 10-20 μF/cm^2,[20] EGOFET responds to changes of potential as low as 50-100 μV[21]. These correspond approximately to a few recognition events per 100x100 nm^2 area of the device. Considering an active channel area $A=W\cdot L$ given by width W multiplied by length L, EGOFET with A=1 mm^2 responds to 10-100 million recognition events occurring on

the device. EGOFETs were shown to transduce signals in neuronal cell populations, sub-nM concentration of neurotransmitters[22] and DNA[23], local pH changes (9mV/pH)[24], penicillin[25] and biotin-streptavidin hybridization[26].

SFS is instead sensitive to a few single antibody-antigen interactions. In SFS, the force dependence on the probe-surface distance, termed force curve, is recorded. A force curve exhibits regions where a smooth variation vs the distance is interrupted by abrupt changes. These "jumps" are interpreted as the rupture of single or multiple bonds that were formed because of molecular recognition interactions. The value of the forces measured by SFS depends on both the loading rate[27,28] and the relevant electrostatic interactions[29]. Being the latter anisotropic, the orientation of the recognition moiety on the surface is important. This orientation may substantially vary depending on the protocol adopted for immobilizing the recognition group on the surface. SFS has been successfully applied to measure the forces between ligands and receptors[30,31], antibody-antigen[32,33], to investigate the unfolding of proteins[34] , protein stability[35], the interaction between carbohydrates[36], and cell adhesion[37].

Here the analytical target is interleukin-4 (IL4), an anti-inflammatory cytokine relevant in several pathologies[38–41]. We adopt IL4 monoclonal antibody as the specific recognition moiety in EGOFET and SFS. Two distinct Ab-immobilization protocols on the gate electrode have been compared. The first is based on 6-aminohexanethiol (HSC6NH2) monolayer activated by glutaraldehyde[42,43]. This functional approach guarantees chemical binding between the metal and the side chains of the lysine residues in the Ab; however, it does not allow one to control the Ab orientation due to the natural abundance of lysine in the Ab backbone. The second strategy exploits the recombinant His-Tagged PG, whose N-terminus side is tailored by a 6-histidine chain (6-His-Tag). His-Tags are well-known to bind polycrystalline Au[44,45]. This

affinity was already exploited for the fabrication of nano-mechanical motors based on the grafting of F1-ATPase on gold substrates[46]. His-Tagged PG forms an oriented layer which promotes Ab immobilization on the Au electrode[47]. Neutron reflectometry, light interferometry and ellipsometry show that Abs on PG-functionalized ideal surfaces form smooth monolayers[48]. Antibodies are oriented by the specific interaction of PG with the fragment crystallizable region (Fc) that forces Ab to expose its binding sites to the environment[49,50].

Our results show a substantial difference in EGOFET and SFS responses to IL-4 when its antibody is immobilized on 6-His-Tagged PG/Au electrodes. EGOFET detects changes of charge mobility and threshold voltage for IL-4 concentrations as low as 5 nM. No change is detected on electrodes functionalized with HSC6NH2. SFS experiments allow us to estimate a larger probability of specific recognition events (P_{sb}≈30%) occurring on PG-functionalized electrodes with respect to the control samples (P_{sb}<10%). Specific binding events display a mean (un-)binding force ≈99 pN, and ≈109 pN for PG- and HSC6NH2-functionalized ones, respectively. The respective dissociation time constants are in the 50:1 ratio. This evidence demonstrates that Ab-Ag pairs with larger conformational stability are more likely formed on PG functionalized electrodes, as a result of higher orientational order of the Ab on PG-functionalized Au electrodes.

These results show the direct correlation between SFS measurements at the single molecule level and the electronic response of the EGOFET that is caused by a change of electrostatic potential on mm^2 channel. The evolution of this approach leads to a methodology for optimization and reproducibility of label-free biosensors.

2. RESULTS AND DISCUSSION

2.1 Electrochemical measurements

The result of the functionalization of Au electrodes was first assessed by cyclic voltammetry and impedance spectroscopy (see Fig. 3) by monitoring the changes in the faradaic response of the ferricyanide redox probe, $[Fe(CN)_6]^{3-/4-}$. In the case of HSC6NH2-functionalized Au electrodes, cyclic voltammetry displays an increase of the peak-to-peak distance from 60 mV to >250 mV upon changing the pH of the solution from neutral to basic values (Fig. 3a). This indicates a dramatic slowing down of the electron transfer, not observed on bare Au, that is consistent with the presence of the amino-terminated SAM on the electrode surface[51].

We monitored PG adsorption onto polycrystalline Au electrodes by means of impedance spectroscopy (Fig. 3b). The data fitted with Randles circuit (see Experimental Section 4.3) show that the capacitance (C_{DL}) decreases from 11.3(±0.2) μF to 2.1(±0.1) μF and R_{CT} increases from 12.8(±0.2) Ω to 270(±3) Ω. This indicates that PG is adsorbed onto Au electrode. The orientation of the adsorbed PG is assessed by measuring the impedance changes upon incubation of the PG-functionalized electrode in a 400 mM imidazole solution for 30 min. We observe a capacitance increase to 2.7(±0.1) μF, along with a dramatic decrease of R_{CT} down to 63(±0.1) Ω. These changes evidence partial desorption of His-Tagged PG from the gold electrode, thus proving that His-Tag mediates the PG assembly on Au (see Fig. 3b).

Both strategies are effective for immobilizing of anti-IL4 on the surface as apparent from Fig. 4 and the data reported in Table S1. For both electrode functionalizations, we observe a significant increase of the charge transfer resistance R_{CT} upon incubation in anti-IL4 solution. The capacitance change is consistent with the Ab adsorption for the HSC6NH2-functionalized

electrode. The capacitance exhibits no significant change in the case of PG-functionalized electrode.

2.2 Tapping mode AFM

The ability of both functionalization protocols to lead to Ab immobilization onto the gold substrate has been evaluated by tapping mode AFM in air and PBS medium. The surface topography of a typical bare gold sample recorded in air is displayed in Fig. 5a. The sample consists of few tens nm-diameter gold grains formed by thermal sublimation, with a maximum height of 10 nm and root mean square (RMS) roughness of 1.1 nm. PG adsorption (Fig. 5b) yields a smoother surface of reduced height and roughness. Incubation of the sample with the anti-IL4 solution leads to an increase of the maximum height by 3.5 nm and roughness by 0.39 nm (Fig. 5c). The height difference is in good agreement with the size of IgG antibodies adsorbed with an orientation consistent with the so-called Y configuration previously reported in air[52].

The RMS roughness for the different functionalization steps (Fig. 5d) follows the same trend both in air and in phosphate buffer solution (PBS). There is a decrease upon PG deposition that is followed by an increase of 0.39 nm in air and 0.61 nm in PBS as a result of the antibody immobilization.

2.3 Single force spectroscopy

After assessing the successful immobilization of anti-IL4 on modified gold substrates, bio-molecular recognition has been studied by means of SFS using probes functionalized with IL-4 linked to the tip by a flexible PEGylated chain (see Experimental Section 4.4). The binding

forces between the specific probe and anti-IL4 bound to the electrode surface were extracted from series of repeated force curves acquired on a 32 x 32 points grid on an area of 1 μm x 1 μm (see Experimental Section 4.4).

Fig. 6a and Fig. 6b show the 2D-histograms containing the number of events with a given unbinding force (F_{ub}) and unbinding length (L_{ub}) for PG- and HSC6NH2-functionalized electrodes, respectively. These histograms cluster together the curves with similar values of the unbinding forces and unbinding distance. Each point (represented as an hexagon) in the 2D histograms contains the force curves corresponding to different types of events. As an example, Fig.s 6c and 6d show a representative force curve for one of the hexagons in Fig.s 6a and 6b. The noisy and adhesive behavior observed in the force curves is related to the fact that the measurements were performed on a real technological surface like polycrystalline gold, instead of prototypical substrates such as mica, which is atomically flat on large areas and more homogenous.

Regarding unbinding lengths, all events occur in the 20-40 nm range with a dispersion ranging from 10 to >50 nm corresponding to the PG-coated Au surface. The most probable unbinding lengths occur in the 10-20 nm range with dispersion ranging from 10 to 35 nm for anti-IL4/HSC6NH2/Au surface. We infer that for PG/Au electrodes unbinding events are more spread out at different lengths, and their unbinding distance is further away from the surface. This observation is consistent with the presence of a larger fraction of oriented antibodies in a standing Y-shape configuration[53], since in this case we expect that the unbinding event take place further away from the surface. Additionally, the Fab fragments of an IgG antibody are linked to the Fc fragment through di-sulphide bonds, resulting in an increased flexibility of these fragments[54]. Thus, an antibody in Y-shape configuration is less constrained by the substrate, hich

explains the broader distribution of unbinding events in distance in the case of highly-oriented anti-IL4. For HSC6NH2 functionalization, our results suggest that the anti-IL4 is randomly oriented.

We then performed a statistical analysis of the large dataset of (un-)binding forces F_{ub}. As shown in Fig.6e, both anti-IL4/PG/Au and anti-IL4/HSC6NH2/Au, along with the crosscheck sample (namely, tip functionalized with IL6 and Au electrode coated with anti-IL4) yield apparently skewed histograms of F_{ub}. This is not surprising because the data sets have been filtered out the aspecific events occurring at $F_{ub} \leq 20$pN. The size of the bin of each histogram is calculated depending on the number of curves N_{SB} in the data set giving rise to (high-force) specific (un-)binding (*SB*). This number changes from sample to sample and therefore the sizes of histograms in Fig. 6 are different. Specifically, the number of bins in each histogram is chosen as N_{bin}=NINT($3.49 \cdot \sigma / N_{SB}^{1/3}$), with NINT being the nearest integer round-off, and σ the standard deviation of the data set. The bin size of each histogram is given by $\Delta F=(F_{max}-F_{min})/N_{bin}$, where F_{max}, F_{min} are the boundary values of the force range measured experimentally. The value of the histogram is normalized to the Specific Unbinding Probability Density (SUPD):

$$(1)\quad SUPD(F_k) \approx 100 \frac{N_{SB}}{N_{TOT}} \left[\frac{1}{\Delta F} \frac{N_k}{N_{SB}} \right]$$

where N_k is the number of curves in the *k-th* bin whose unbinding force F_{ub} falls within $F_k \pm \Delta F/2$. Its integral vs F_{ub} across the data set is estimated as the summation on the histogram bins multiplied by ΔF. The summation index runs from 1 to k_{max}, k_{max} being the index corresponding to $F_{kmax}(F_{ub})$. The Specific Unbinding Probability SUP(F_{max})=$100 \cdot N_{SB} / N_{TOT}$ is the asymptotic limit of the curves shown in Fig. 6f:

$$(2)\ SUP(F_{ub}) = \int_0^{F_{ub}} SUPD(F)dF \approx 100\left[\sum_{k=1}^{k_{\max}} \frac{N_k}{N_{TOT}}\right]$$

The skewness (standardized third moment) of each data set is found to be significant as its values largely exceed the corresponding Gaussian distribution estimator $\sqrt{6/N_{SB}}$ [55]. The three data sets exhibit a mean force value $\left\langle F_{ub}^{*}\right\rangle(\pm\sigma)$ equal to 98(±55) pN, 109(±59) pN and 80(±39) pN for PG, HSC6NH2, and crosscheck samples respectively. We have inserted these values as parameters in the functional[56,57],

$$(3)\qquad SUPD(F_{ub}) = 100\cdot\frac{N_{SB}}{N_{tot}}\cdot\chi^2\left(F_{ub}\right) = 100\cdot\frac{N_{SB}}{N_{tot}}\frac{1}{2^p\Gamma(p)}\left(\frac{\sqrt{p}\cdot F_{ub}}{\sigma}\right)^{p-1}\exp\left(-\frac{\sqrt{p}\cdot F_{ub}}{\sigma}\right)$$

Eq. 3 describes a chi-square distribution normalized to the overall probability to detect a specific (un-)binding event. Here the parameters are: $p=\left(\frac{\left\langle F_{ub}^{*}\right\rangle}{\sigma}\right)^2$, $\Gamma(p)$ is the gamma function. The trends of SUPD, depicted as continuous curves overlapping the histograms in Fig. 6e, show a conformational adherence within the force range from 20 pN to 300 pN[58–62]. It is clear that the SUPD curves for both PG and HSC6NH2 are alike, and can be mapped one onto another by a simple vertical rescaling. On the other hand, they are substantially different from the one of crosscheck sample that has the same shape but whose peak is displaced at lower force values, and they are radically different from the one of the control sample (bare Au) that does not exhibit an apparent skewness. By looking at the SUP it is clear that anti-IL4/PG/Au induces a three-times larger frequency of specific binding events than the sample anti-IL4/HSC6NH2/Au (see Fig.6f). These values can be interpreted as the result of the effective coverage of functional Abs on the respective surfaces, viz. PG yields a 30% coverage of available Abs for recognition of

IL4, whereas HSC6NH2 only 10%. The comparison between the two immobilization strategies has been reproduced with another antibody-antigen pair, viz. interleukin-6 (IL-6)/anti-IL6 pair, yielding even more marked differences in recognition probability (see Fig.S5 Supporting Information). Noticeably, the SUP of HSC6NH2 is comparable to that of crosscheck sample, although it appears that the latter is contributed to events whose force is below 200 pN. This implies that in the crosscheck sample it is possible to observe single specific recognition events, but not multiple ones, conversely to the other cases. The distribution related to bare gold shows a different trend, and the SUP is much lower than all the other distributions. This means that IL4 poorly interact with un-functionalized Au, as expected.

In order to gain insights into the energy landscape of the bound complexes, we carried out experiments at different retraction velocities. According to the Bell-Evans model, the force of a single-energy barrier in the thermally activated regime scales up with the logarithm of the loading rate[28] (see Supporting Information 4.4):

$$(4) \qquad F_{ub} = \frac{k_B T}{x_\beta} \ln\left(\frac{v x_\beta}{k_{off} k_\beta T}\right)$$

Here F_{ub} is the most probable unbinding force, v the loading rate, x_β the position of the energy barrier along the reaction coordinate, k_{off} is the dissociation constant at zero force and k_BT is the thermal energy.

The associated values for the Bell-Evans model parameters such as the reaction length x_β and the lifetime of the complex $\tau=1/k_{off}$ are reported in Table II. The value of the k_{off} =4*10^{-3} s^{-1}, corresponding to τ=206 s for PG-based functionalization, is in good agreement with the values observed in literature for specific antigen-antibody pairing characterized by single molecule force spectroscopy[58,63]. For HSC6NH2-functionalization, we obtain k_{off} =0.209 s^{-1}, corresponding

to a lifetime τ=4.78s. The almost two orders of magnitude ratio of the k_{off} indicates that the antigen fits more steadily the antibody when the latter is immobilized onto the PG substrate, as compared to the HSC6NH2-functionalization[64,65]. This yields the increased binding affinity between IL4/anti-IL4 when PG is used for the antibody immobilization. As far as the potential barrier width between the bound complex and the transition state, x_β, is concerned, the values for both functionalization approaches fall in the range usually found for specific interactions between partners with a rather high conformational stability[53]. We observe that the IL4/anti-IL4 complex formed via PG immobilization with a lifetime of the complex of 206s shows higher stability as compared to the one formed onto the SAM-functionalized surface, which will dissociate faster at a complex lifetime of 4.78s.

According to the Evans Bell model, the dissociation of the antibody-antigen complex under an external force is described in the frame of the transition state theory[27,66]. One k_{off} is calculated, ΔG can be estimated using the following equation, where h is Planck's constant:

$$\Delta G = -k_B T \ln \frac{k_{off} \cdot h}{k_B T} \quad (5)$$

The total free energy of the antibody-antigen complex has been estimated for the two gold functionalization approaches, obtaining values of -91 kJ/mol for the PG mediated functionalization and -82 kJ/mol for the HSC6NH2-functionalization. One should take into account the fact that this free energy includes contribution from the unbinding process of the antibody-antigen complex, as well as from the stretching of the PEG linker. Therefore, the free energy related exclusively to the unbinding process of the IL4/anti-IL4 complex can be calculated from this expression:

$$\Delta G_{ub} = \Delta G_{Ab/Ag} - \Delta G_{PEG} \quad (6)$$

The free energy related to the stretching of a 10 nm long PEG linker has been estimated experimentally to be -7.45 kJ/mol[67], so the unbinding free energy corresponding to the antibody-antigen pairs are -84(±42) kJ/mol for the PG-based functionalization and -75(±26) kJ/mol for the HSC6NH2 functionalization. These values of the unbinding free energy could be related to the breaking of several hydrogen bonds and one or two salt bridges that are responsible of the Ab-Ag recognition.

2.4 Detection of IL4 with EGOFET-based immunosensors

The pristine device exhibits a field-effect charge mobility μ=3.8×10^{-4} cm^{2}V^{-1}s^{-1} and a threshold voltage V_{th}=-40mV. The leakage current is always lower than 10nA along with an almost negligible hysteresis featuring no electrochemical doping of pentacene thin-film.

The I-V characteristics of an immuno-EGOFET with a gate electrode modified with anti-IL4, immobilized by glutaraldehyde-based protocol, is shown in Fig. 7a. We observe that the anti-IL4 (red curve) induces an electrical change in the I-V curve with respect to that recorded before anti-IL-4 immobilization (black curve). The Au gate electrode was then incubated in a reference solution of IL-4 at a concentration of 5nM. This additional exposure does not give rise to further electrical change (blue curve). According to the protocol of Porter et al.[68,69], the biological layer has been electrochemically detached (see Fig. S4 in supporting info) via the cleavage of the chemical bond between Au and sulphur of the 6-aminohexanethiol. The subsequent increase of the EGOFET performance proves that no deterioration is taking place at the experimental time-scale. The same validation process has been applied to the PG-based protocol (see Fig. 3b). At

variance with the previously described case, a significant change in the electrical response is now observed after incubation of the gate electrode in the IL-4 solution.

We then focused our attention only on the PG-mediated functionalization and monitored step-by-step changes in the electrical performances of the device by recording shifts of μ and V_{th} (see Fig.7c and Fig.7d). Throughout the functionalization procedure, mobility shows a gradual decrease down to 60% of the initial value. This is ascribed to a decrease of the capacitive coupling between the gate electrode and the organic semiconductor thin film due to addition of biological layers on the gate surface (see Fig. 7c). Regarding the threshold voltage, a rather complex behavior has been observed. On one hand, the adsorption of protein G gives rise to a negative shift of threshold voltage, while on the other hand both anti-IL4 grafting and subsequently IL-4 recognition yield an opposite shift. This means that the protein G reduces the charge-carrier density in the conductive channel with respect to bare Au electrode. Owing to the fact that the isoelectric point (pI) of protein G is acidic (around 5), this means that protein G is negatively charged at pH=7.2 and strongly coupled to the charge carriers in the channel to act as a trap, and not as a dopant. In the case of IL-4 whose pI=8.2, there is a partial release of these "trapped" carriers manifesting itself with a shift towards less negative threshold voltage. This can be due either to formation of a surface dipole upon specific binding of IL-4 to its anti-IL4, thus increasing the capacitance of the interface and the consequent capacitive coupling, or to a partial compensation of the negative charge density of protein G.

Our electrical measurements show that PG functionalized EGOFETs are capable to sense IL4 down to 5 nM concentrations, while the HSC6NH2 functionalized device does not give a measurable response. Protein G functionalized device shows a mobility loss of 16% and a positive shift in the threshold voltage of approximately 10 mV after exposure to an IL-4 solution

(see Table I). The absence of significant changes in the electrical properties EGOFETs with gate electrodes modified with the HSC6NH2-based functionalization is consistent with the much lower probability of recognition events for randomly oriented anti-IL4.

3. CONCLUSIONS

The detection of the bio-molecular recognition between interleukin-4 and its specific antibody by electrolyte-gated organic field-effect transistor and force spectroscopy measurements involves different processes, spatial and temporal scales. While EGOFET detection involves change of electrostatic charge due to about 10^{12} local recognition events per cm^2, SFS involves the detection of a few biorecognition events occurring at nm length-scales. For this reason, comparing and complementing the results acquired with the two techniques is a challenging task whose correlation is not trivial. We have successfully merged the evidences obtained by electrical and mechanical techniques to comparatively assess two immobilization protocols for anti-IL4 on polycrystalline Au. The success of EGOFET in detecting nanomolar concentrations of IL4 in the case of protein G mediated Ab immobilization correlates with the larger areal density of available anti-IL4 antibodies as evidenced by SFS measurements, corresponding to 30% coverage with respect to just 10% in the case glutaraldehyde-based immobilization. While there is no substantial difference in the distribution of the specific binding force for the two immobilization schemes, there is a marked difference in the kinetic constants, that show a longer average lifetime of the antibody-antigen complex, τ = 206(±103) s, and a closer bond, x_β = 3.2(±0.2) nm, for the anti-IL4/PG/Au. This shows that the local environment of the available antibodies, which is subtly affected by the density and orientation of other antibodies, is important in determining the effectiveness of the local recognition event. Our comparative study demonstrates that the optimum antibody functionality towards its antigen is

achieved for the PG-mediated anchoring and that achieving this high density of available antibodies is crucial for enhancing the label-free detection of the relevant protein.

4. EXPERIMENTAL METHODS

4.1. Device fabrication

Our devices are prepared onto gold-coated glass slides purchased from Phasis (Switzerland). These substrates are made of quartz glass (1mm thick) and a gold layer of 50nm plus few nm of titanium as adhesive layer. Each test-pattern bears 4 transistors, whose channel length is 15μm and channel width equal to 27000 μm. The fabrication is carried out by laser ablation with a short-pulsed Nd:YAG infrared (IR)-laser supplied by a laser scan marker (Scriba Nanotecnologie S.r.l., Bologna, Italy). The IR-Laser pulse frequency and intensity are optimized in order to find the best compromise between removal of the Au layer and roughening of the underlying quartz. Typical operation is performed at a laser power of 8300W and a pulse of 10ns and a frequency of 15500Hz. The laser focus is moved over the surface at a scan-rate of 2000μm/s. Details are described elsewhere[70].

4.2. Gate functionalization

6-aminohexanethiol (HSC6NH2) and glutaraldehyde are purchased from Sigma-Aldrich and used without further purification. Recombinant PG, monoclonal anti-murine IL-4 (Anti-IL4), and recombinant murine IL-4 were purchased from Vinci-Biochem S.r.l. (Firenze, Italy). These biological species are produced by Biovision (San Francisco, USA). His-Tagged recombinant protein G lacks the albumin and cell membrane binding domains.

The gate electrode is a polycrystalline Au wire (diameter equal to 1mm). First, this electrode undergoes a standard cleaning procedure[71]: (i) immersion in a concentrated H_2SO_4 at 100°C for 1h; (ii) 20 cycles of electro-polishing by sweeping the potential from 0V to 1.5V in H_2SO_4 (1M). The glutaraldehyde-based functionalization occurs by immersing the gate electrode in a 6-aminohexanethiol solution (1mM) overnight. The further activation is achieved by using glutaraldehyde solution (2.5%v/v) for 1h at 5°C and then the functionalized electrode is immersed in an antibody solution (0.25mg/ml anti-IL4) for 1h at 5°C. The last step consists of immersing the Ab-coated electrodes in buffer solution (100mM of PBS, pH 7.4) IL-4 (5nM). The other functionalization exploits a buffer solution (100mM of PBS pH 7.4) of protein G (5mg/ml). Ab and Ag solutions are the same of the previous protocol.

4.3. Electrical measurements

All the electrochemical, morphological and mechanical investigations described so far proved the possibility of successfully immobilizing anti-IL4 antibodies on functionalized gold surfaces. SFS experiments have also suggested that the use of PG-based immobilization protocol significantly enhances the probability of recognition events between the surface coated with anti-IL4 and IL4. We then applied these immobilization strategies to the functionalization of the gate Au electrode of EGOFETs to obtain an immunosensor. Our aim is to establish the minimum detection level of IL4 in test solutions, and assess whether these concentration ranges are comparable with biologically-relevant ones. We compared the electrical responses of EGOFETs with gate electrodes functionalized with the different protocols to assess whether controlling the orientation of the Abs on the surface would enhance the sensing capability of the immunosensors.

All the electrical measurements were performed with home-built EGOFETs. As mentioned in the experimental methods (4.1), the electronic transducer was fabricated by means of laser ablation[70]. Particular attention has been paid to maximize the *W*/*L* ratio, which is the geometrical parameter scaling the drain-source current (I_{DS}). This home-built EGOFET has been operated in a buffer solution (100mM of PBS at pH 7) mimicking the physiological conditions. The buffer solution has been confined on top of the electronic transducer by means of a PDMS pool, as shown in the cross-section of Fig.1.

Source, drain and gate electrodes were connected to a Keithley 2612 Source Meter. The electrical response was acquired by means of a probe station. All the electrical measurements were carried out in ambient atmosphere. The I-V transfer characteristics were performed by sweeping the gate-source voltage (V_{GS}) from +0.2 V to -0.5 V while leaving the drain-source voltage constant at -0.5V (saturation regime) for the reference device. The I-V output characteristics were carried out by sweeping drain-source voltage (V_{DS}) from 0 V to -0.5 V and V_{GS} from 0 V to -0.5 V with step of 0.1 V. The V_{GS} scan rate is 20mV/s and 80mV/s for transfer and output characteristics respectively.

Electrochemical measurements are performed by an usual three-electrodes cell connected to a potentiostat/galvanostat μ-Autolab type III (Metrohm Italiana S.r.l., Varese, Italy), using a polycrystalline Au wire, as working electrode, functionalized with the above-mentioned protocols; a Pt sheet and Ag/AgCl were used as counter and reference electrodes respectively.

The impedance response is fitted by Randles circuit, which is an equivalent circuit composed by an electrolyte solution resistance, R_S, a charge transfer resistance, R_{CT}, a Debye-Helmhotz capacitance, C_{dl} and a Warburg element, W.

4.4. Single molecule force spectroscopy measurements

In these experiments, the force dependence on the probe-surface distance is recorded (viz. force curve). A force curve contains regions that show a smooth variation with the distance. Those regions are interrupted by the presence of sharp changes in the force, which are associated with molecular recognition interactions, interpreted as the rupture of one or several bonds. The forces measured by force spectroscopy are dynamic in nature, as they depend on the loading rate[27,28] and electrostatic interactions[29]. To certain extent, the electrostatic interactions are controlled by the immobilization protocols applied to a bio-specie of interests on a certain substrate.

4.4.1. Tip functionalization

Phosphate buffer saline powder which yields 0.01 M phosphate buffered saline (NaCl 0.138 M; KCl 0.0027 M) when dissolved in 1 liter of water, hydrogen peroxide 30%, sulphuric acid, 3-aminopropyl-triethoxysilane (APTES), glutaraldehyde 8%, 6-aminohexanethiol and ethanol were purchased from Sigma Aldrich. The 24-unit ethyleneglycol functionalized with succinimidyl and maleimido ends (NHS-PEG_{24}-Mal) and the sulfhydryl addition kit containing: SATA (*N*-succinimidyl-S-acetylthioacetate),hydroxylamine•HCl, conjugation buffer stock (10X), dimethylformamide and Dextran desalting column were purchased from Thermo Scientific. Recombinant protein G, monoclonal anti-murine IL-4 and recombinant murine IL-4 are produced by Biovision (San Francisco, USA).

AFM silicon nitride tips were first cleaned thoroughly by immersion in a piranha solution (3:1 concentrated sulfuric acid to 30% hydrogen peroxide solution) for 30 minutes. They were then rinsed with nanopure water and dipped into a solution of 3-aminopropyl-

triethoxysilane:water:ethanol (ratio 5:5:95 v/v) for 30 minutes. Finally, the amino-functionalized tips were rinsed with nanopure water, ethanol and nitrogen dried.

Next, the heterobifunctional NHS-PEG_{24}-Mal linker was reacted with the antigen bearing a sulfhydryl group. Prior to that, free sulfhydryl functionality was added to the antigen using the SATA reagent. A 17.3 mM SATA solution in DMF was added in 10-fold molar excess to 1 mL of protein. The reaction was incubated for 30 minutes at room temperature. Then, 5 mg Hydroxylamine·HCl was mixed with 100 µl Conjugation Buffer Stock (10X). To de-protect the latent sulfhydryl, 100 µl of hydroxylamine solution was added to the SATA-modified protein and the mixture was incubated for 2 hours at room temperature. The de-protected sulfhydryl protein was then added to the equilibrated desalting column to remove non-reacted reagents. The maleimide conjugation buffer was added to the desalting column and 1 mL fractions were collected and the absorbance of each fraction was measured at 280 nm to locate the protein. Fractions containing most of the protein were then reacted with the NHS-PEG_{24}-Mal linker. A 10-fold molar excess of the PEG linker was incubated with the sulfhydryl-modified antigen at 4°C for 12 hours. Finally, the amino-functionalized AFM tips were immersed in the PEG-antigen solution for 2 hours at room temperature. The tips were when rinsed with PBS 0.1 M and stored in a Petri dish at 4°C until further usage.

4.4.2. Substrate functionalization

The substrates used were mica sheets covered with a 3 nm adhesive Cr layer and a 50 nm thick gold layer. The antibody immobilization onto the gold substrate has been performed by following the same protocols used for the gate functionalization (section 4.2).

4.4.3. Topography measurements

Tapping mode AFM was employed to record topographical images of the samples at different functionalization steps in both air and PBS[72]. Rectangular PPP-NCH (Nanoworld AG, Switzerland) cantilevers with a nominal force constant k= 40 N m^{-1} and a resonant frequency of 291 kHz have been used for air measurements. As for the experiments in liquid environment, rectangular OMCL-RC800PSA (Olympus, Japan) with a nominal force constant of 0.4 N/m and a resonant frequency of 33 kHz were employed. The topography measurements were performed in amplitude modulation AFM by driving mechanically the cantilever[73].

4.4.4. Single molecule force spectroscopy measurements

Single molecule force spectroscopy experiments were performed with a Multimode atomic force microscope fitted with a Nanoscope V controller (Brucker, Santa Barbara). The microscope is equipped with a liquid cell where approximately 60 µl of PBS 0.01M pH= 7.4 are introduced in order to carry out the measurements. Triangular silicon nitride tips OTR-4 (Brucker, Santa Barbara) with a spring constant of 0.015 – 0.08 N/m and resonant frequency of 1.8 kHz and 8 kHz were used. The force constant and quality factor are determined by using the thermal noise method[74] . At the end of each experiment, the optical lever sensitivity was calibrated by acquiring deflection versus distance curves on a hard surface (mica). Typically 100 deflection *vs* distance curves are acquired and the sensitivity of the photodiode is calculated as the mean value. The force is calculated using Hooke´s law: $F = -kd$ (d= cantilever deflection, k=cantilever force constant). The applied force was maintained below 600 pN.

The force curves were acquired in static mode by approaching and retracting the tip toward the sample by 200 nm at different velocities (0.5, 1, 2 and 5 Hz). Each time, the tip was kept in contact with the sample for 0.5 s in order to favor the recognition process.

Several rounds of control experiments have been performed to check the specificity of the unbinding events. On one hand, force curves of a bare AFM tip interacting with the substrate at each functionalization step for both protocols were recorded. Afterwards, antigen tethering AFM tips were tested against Au, anti-IL4/HSC6NH2/Au and anti-IL4/PG/Au. On the other hand, cross-reactivity experiments have been performed by bringing IL4 antibodies on the substrate in contact with the IL6 antigen on the tip.

4.5 Dynamic force spectroscopy data analysis

A total of 16297 force distance curves were analyzed by using customized software in an automated way. The curves were averaged and the contact point was set according to a deflection threshold. Event recognition was based on the values of the second and third derivatives of the deflection; the event was labeled as a recognition event whenever the derivatives were found to be above a threshold with respect to the noise level. An algorithm was created to discriminate specific recognition events from surface adhesion events. The algorithm is based on the calculation of the deviation between the deflection curve and the straight line that goes from the peak minimum to the contact with the surface (see Supporting Information 4.5). Tables containing information on specific events for all the experiments were processed and 1D and 2D histograms were extracted. 1D histograms have been normalized to the number of force distance curves for every set of experiments. 2D histograms represent the number of specific events that occur which a given binding length and a given binding force. The binning sites for the binding length and force where set to 3 nm and 13 pN respectively.

The dynamics of the IL4 antibody-antigen binding was explored by determining the unbinding force as a function of the unbinding rate. The loading rate is the product between the retract

velocity and the spring constant. To account for the contribution of the PEG linker spring constant to the overall spring constant of the system, the loading rate was extracted from the slope of the force curve before unbinding occurs. The plots in figure S5 display the linear increase of the most probable unbinding force with the logarithm of the loading rate for the two antibody immobilization protocols. This characteristic behavior for a thermally activated dissociation process under an applied load has been previously observed for other antibody-antigen complexes.

To determine the kinetic parameters of the molecular recognition process, the length of the energy barrier, x_β, was determined from the slope of linear fit of the unbinding forces vs. loading rate logarithm plot (see Eq.1). Next, the kinetic off-rate constant of dissociation at zero force was calculated by extrapolation to zero forces. Antibody-antigen complexes have limited lifetimes, which are shortened by thermal activation under an applied force. The characteristic time needed for the spontaneous dissociation, τ, is given by the inverse of the kinetic off-rate constant and can be correlated with the specificity of the recognition process as well as the stability of the complex.

5. FIGURES

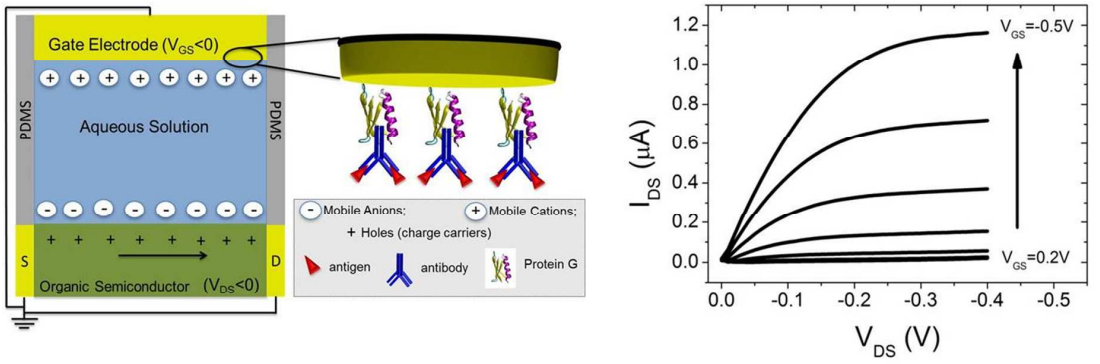

Figure 1 On the left, a schematic EGOFET cross-section along with a sketch of the magnification of the gate/electrolyte interface. On the right, I-V output characteristics of a reference device.

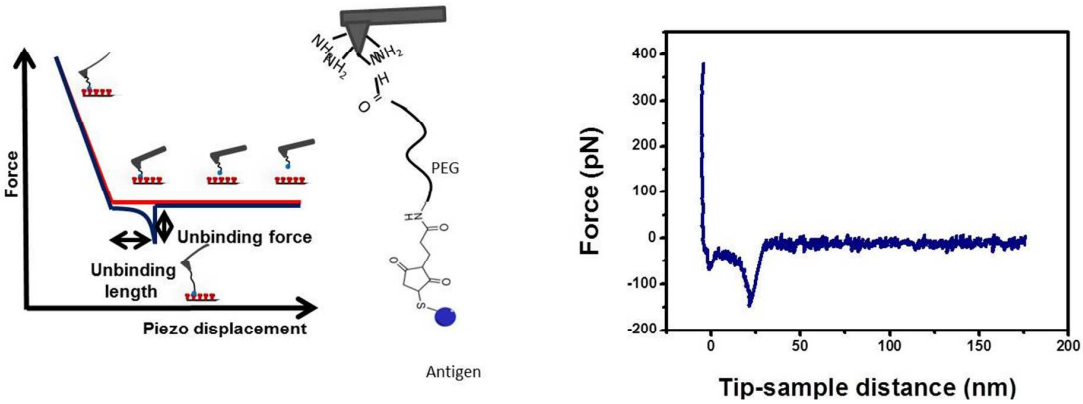

Figure 2. (Left) Schematics of a force-distance plot (force curve). As the tip approaches the sample, as contact is established the repulsive forces cause the tip to bend upwards (red line). The tip is then retracted (blue line). If a recognition event occurs, adhesion forces will make the tip to bend downward during retraction. When force gradient exceeds the spring constant of the cantilever, the probe jumps out of contact to its initial position. The unbinding force of the antibody-antigen pair is the maximum adhesive force, estimated as the vertical difference between the baseline and the minimum force at retraction. Unbinding length is the difference between the tip-sample distance where the unbinding event occurs and the contact point. Discrimination of specific and unspecific binding events relies on the estimate of the gradient of the force near the detachment point. Details are found in Supporting Information. (Center) Scheme of the AFM tip functionalization. IL-4- PEG linker complex is attached to an amino-functionalized AFM tip. (Right) Real force curve shows a specific unbinding event.

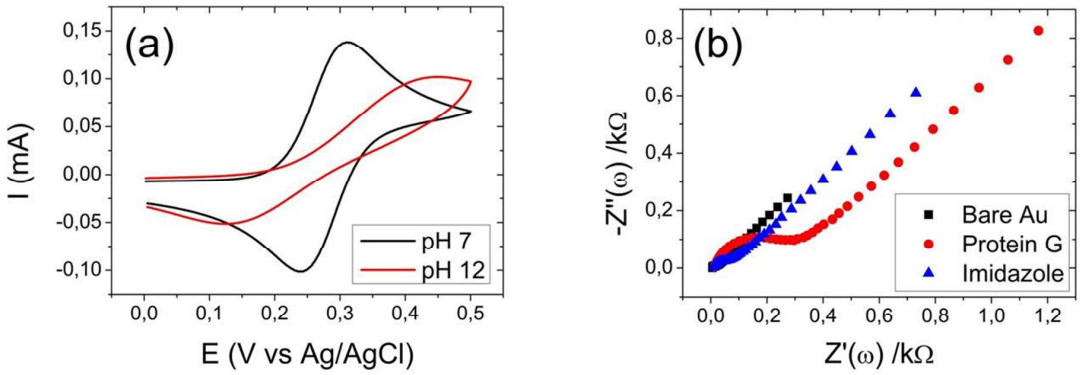

Figure 3 (a) Cyclic voltammograms of the ferricyanide signal at neutral and basic pH at a polycrystalline gold electrode functionalized with HSC6NH2. **(b)** Impedance spectroscopy for bare Au (black filled squares), PG adsorption (red filled circles) and PG elution mediated by imidazole exposure (blue filled triangles).

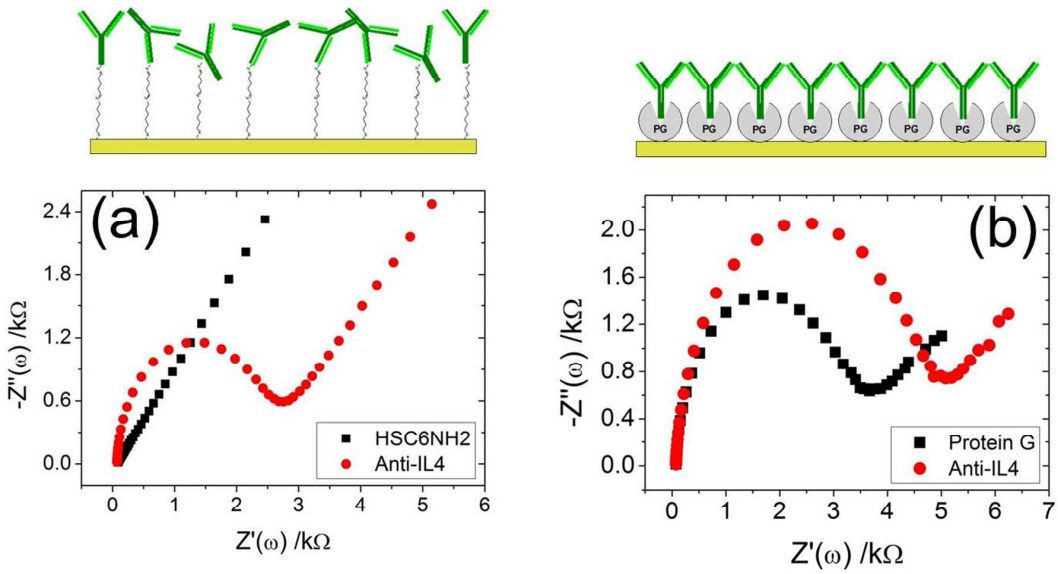

Figure 4 Nyquist plots of **(a)** HSC6NH2- and **(b)** PG-mediated treatment. On the upper part of these plots, a cartoon of the two functionalization strategies is shown.

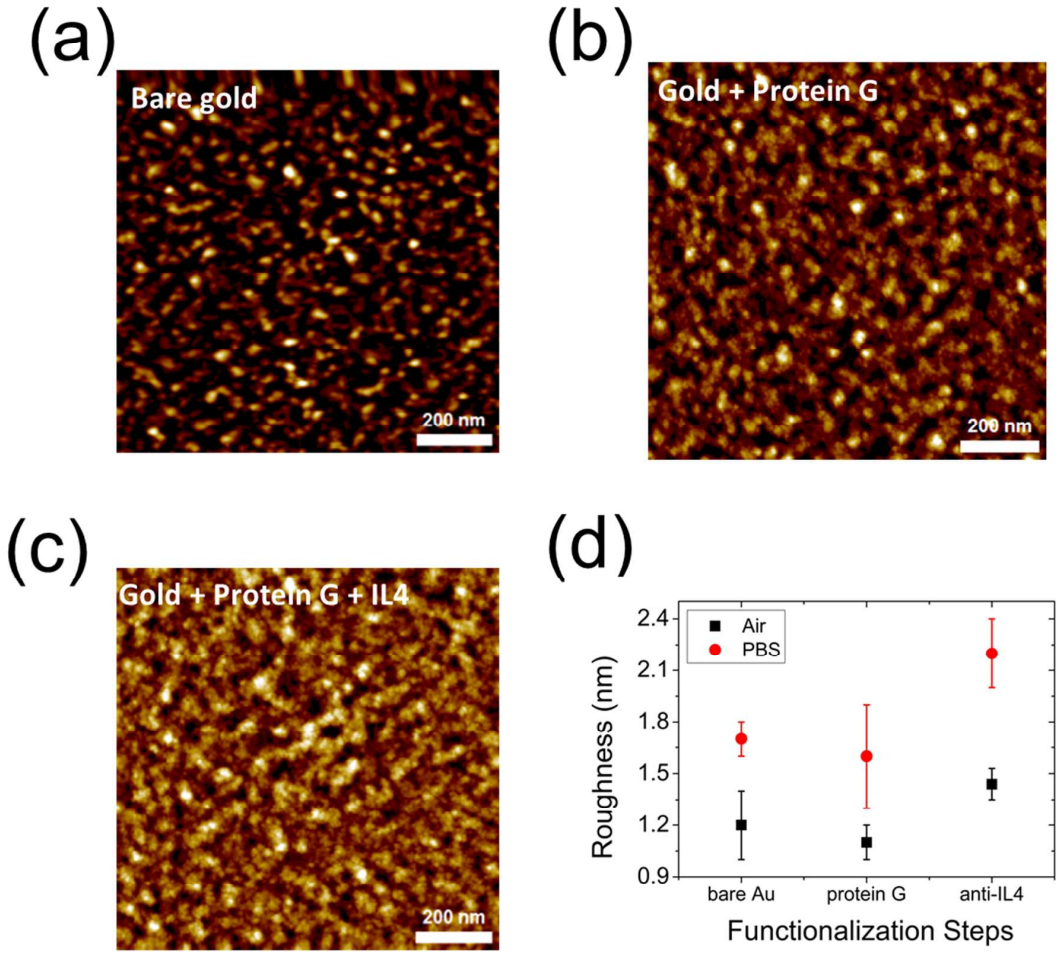

Figure 5 AFM images on bare gold **(a)**, PG-coated gold **(b)**, PG/Anti-IL4-coated gold **(c)**. Roughness data are overlaid in air and in PBS solution **(d)**.

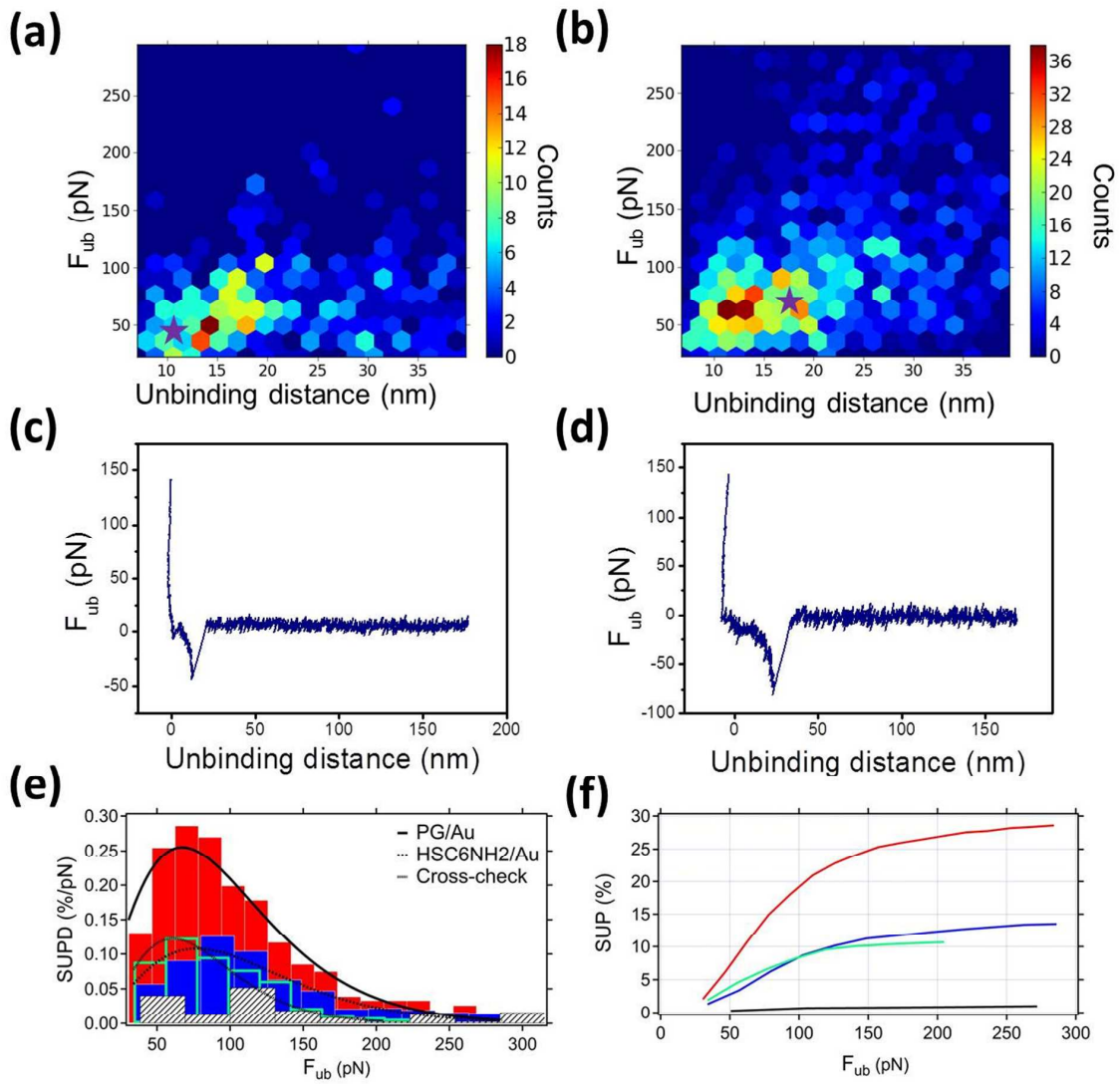

Figure 6 2D histograms of the unbinding distance and unbinding force for **(a)** GA-based protocol and **(b)** PG-based one. **(c-d)** Two representative Force vs distance curves corresponding to the starred hexagons in **(a)** and **(b)**. **(e)** Histograms of SPBD as a function of F. Red, blue, empty and white-black patterned bars stand for PG, GA, cross-check and bare Au respectively. Solid, dashed and dotted lines are the best χ-square fits corresponding to PG, GA and cross-check **(f)** SUP vs. F plots are shown for each protocol.

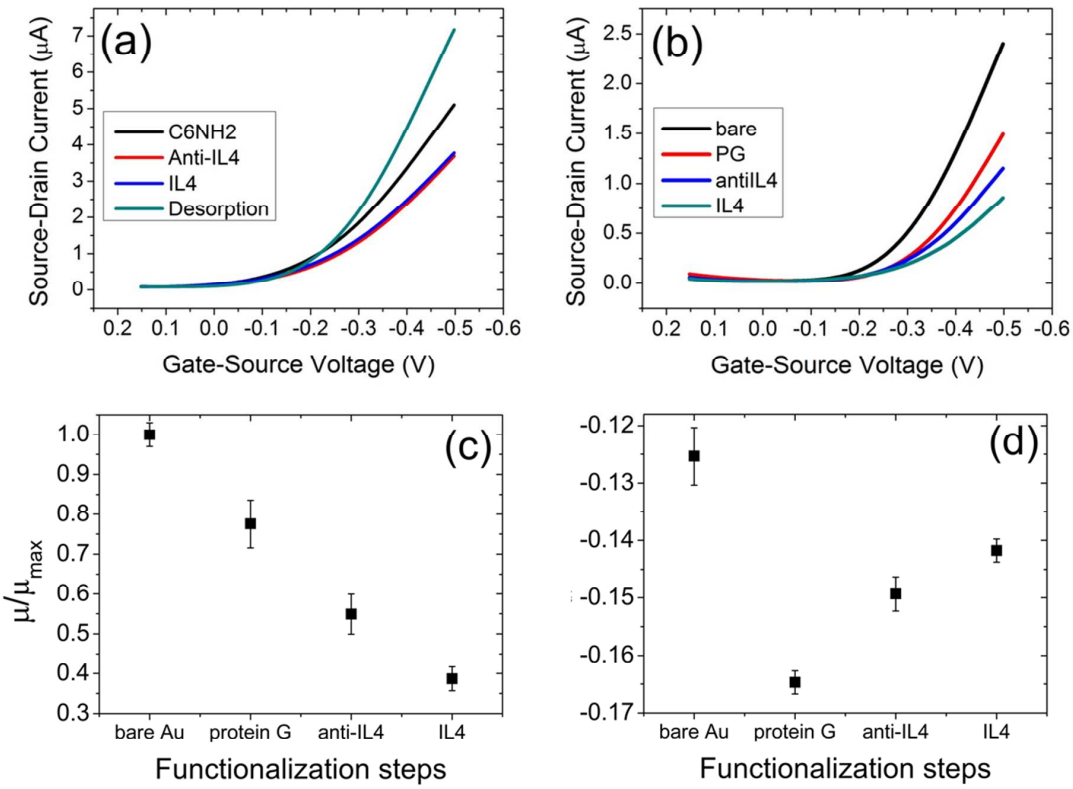

Figure 7 I-V transfer characteristics for **(a)** HSC6NH2- and **(b)** PG-based protocols. Normalized mobility ratio **(c)** and threshold voltage **(d)** trends corresponding to the stepwise functionalization.

Table 1

Experiment	x_β (Å)	k_{off} (s^{-1})	τ (s)	$\Delta G_{binding}$ (kJ/mol)	μ (% loss)	ΔV_{th} (mV)
IL4 on Protein G	3.2(±0.2)	0.004(±0.002)	206(±103)	84(±42)	16	≈10
IL4 on Glutaraldehyde	2.4(±0.1)	0.209(±0.073)	5(±2)	75(±26)	-	-

AUTHOR INFORMATION

Corresponding Authors

*Dr. Stefano Casalini, stefano.casalini@unimore.it

*Prof. Ricardo Garcia, r.garcia@csic.es

Funding Sources

This work was supported by the EU-project I-ONE-FP7 "Implantable Organic Nano-Materials" NMP4-SL-2012, grant agreement n.280772.

ACKNOWLEDGMENT

We thank Prof. Francesco Zerbetto, Alma Mater-Università di Bologna, for useful discussions.

REFERENCES

(1) Mariuzza, R. A.; Immunologie, D.; Pasteur, I.; Cedex, P. THE STRUCTURAL BASIS OF ANTIGEN-ANTIBODY RECOGNITION. *Annu. Rev. Biophys. Biophys. Chem.* **1987**, *16*, 139–159.

(2) BK, V. W.; A.H.W.N., S. Immunoassay Using Antigen-Enzyme Conjugates. *FEBS Lett.* **1971**, *15*, 232–236.

(3) Marquette, C. a; Blum, L. J. State of the Art and Recent Advances in Immunoanalytical Systems. *Biosens. Bioelectron.* **2006**, *21*, 1424–1433.

(4) Hock, B. Antibodies for Immunosensors a Review. *Anal. Chim. Acta* **1997**, *347*, 177–186.

(5) Kurosawa, S.; Park, J.-W.; Aizawa, H.; Wakida, S.-I.; Tao, H.; Ishihara, K. Quartz Crystal Microbalance Immunosensors for Environmental Monitoring. *Biosens. Bioelectron.* **2006**, *22*, 473–481.

(6) Butt, È.; Skla, P.; Raiteri, R.; Grattarola, M. Micromechanical Cantilever-Based Biosensors. *Sensors and actuators* **2001**, *79*, 115–126.

(7) Guilbault, G. G.; Amia, F. Recent Developments in Piezoelectric Immunosensors* A Review. *Analyst* **1994**, *11*, 2279–2282.

(8) Abdulhalim, I.; Zourob, M.; Lakhtakia, A. Surface Plasmon Resonance for Biosensing: A Mini-Review. *Electromagnetics* **2008**, *28*, 214–242.

(9) Lee, C.-S.; Kim, S. K.; Kim, M. Ion-Sensitive Field-Effect Transistor for Biological Sensing. *Sensors* **2009**, *9*, 7111–7131.

(10) Liang, K.; Mu, W.; Huang, M.; Yu, Z.; Lai, Q. Interdigitated Conductometric Immunosensor for Determination of Interleukin-6 in Humans Based on Dendrimer G4 and Colloidal Gold Modified Composite Film. *Electroanalysis* **2006**, *18*, 1505–1510.

(11) Yang, L.; Li, Y.; Erf, G. F. Interdigitated Array Microelectrode-Based Electrochemical Impedance Immunosensor for Detection of Escherichia Coli O157 : H7. *Anal. Chem.* **2004**, *76*, 1107–1113.

(12) Hays, H. C. W.; Millner, P. a.; Prodromidis, M. I. Development of Capacitance Based Immunosensors on Mixed Self-Assembled Monolayers. *Sensors Actuators B Chem.* **2006**, *114*, 1064–1070.

(13) Wan, Y.; Su, Y.; Zhu, X.; Liu, G.; Fan, C. Development of Electrochemical Immunosensors towards Point of Care Diagnostics. *Biosens. Bioelectron.* **2013**, *47*, 1–11.

(14) Casal, P.; Wen, X.; Gupta, S.; Nicholson, T.; Wang, Y.; Theiss, A.; Bhushan, B.; Brillson, L.; Lu, W.; Lee, S. C. ImmunoFET Feasibility in Physiological Salt Environments. *Philos. Trans. A. Math. Phys. Eng. Sci.* **2012**, *370*, 2474–2488.

(15) Palazzo, G.; De Tullio, D.; Magliulo, M.; Mallardi, A.; Intranuovo, F.; Mulla, M. Y.; Favia, P.; Vikholm-Lundin, I.; Torsi, L. Detection Beyond Debye's Length with an Electrolyte-Gated Organic Field-Effect Transistor. *Adv. Mater.* **2014**, 1–6.

(16) Sheehan, a. D.; Quinn, J.; Daly, S.; Dillon, P.; O'Kennedy, R. The Development of Novel Miniaturized Immuno-Sensing Devices: A Review of a Small Technology with a Large Future. *Anal. Lett.* **2003**, *36*, 511–537.

(17) Campana, A.; Cramer, T.; Simon, D. T.; Berggren, M.; Biscarini, F. Electrocardiographic Recording with Conformable Organic Electrochemical Transistor Fabricated on Resorbable Bioscaffold. *Adv. Mater.* **2014**, *26*, 3874–3878.

(18) Cramer, T.; Chelli, B.; Murgia, M.; Barbalinardo, M.; Bystrenova, E.; de Leeuw, D. M.; Biscarini, F. Organic Ultra-Thin Film Transistors with a Liquid Gate for Extracellular Stimulation and Recording of Electric Activity of Stem Cell-Derived Neuronal Networks. *Phys. Chem. Chem. Phys.* **2013**, *15*, 3897–3905.

(19) Khodagholy, D.; Doublet, T.; Quilichini, P.; Gurfinkel, M.; Leleux, P.; Ghestem, A.; Ismailova, E.; Hervé, T.; Sanaur, S.; Bernard, C.; *et al.* In Vivo Recordings of Brain Activity Using Organic Transistors. *Nat. Commun.* **2013**, *4*, 1–7.

(20) Cramer, T.; Kyndiah, a.; Murgia, M.; Leonardi, F.; Casalini, S.; Biscarini, F. Double Layer Capacitance Measured by Organic Field Effect Transistor Operated in Water. *Appl. Phys. Lett.* **2012**, *100*, 143302.

(21) Cramer, T.; Campana, A.; Leonardi, F.; Casalini, S.; Kyndiah, A.; Murgia, M.; Biscarini, F. Water-Gated Organic Field Effect Transistors – Opportunities for Biochemical Sensing and Extracellular Signal Transduction. *J. Mater. Chem. B* **2013**, *1*, 3728–3741.

(22) Casalini, S.; Leonardi, F.; Cramer, T.; Biscarini, F. Organic Field-Effect Transistor for Label-Free Dopamine Sensing. *Org. Electron.* **2013**, *14*, 156–163.

(23) Kergoat, L.; Piro, B.; Berggren, M.; Pham, M.-C.; Yassar, A.; Horowitz, G. DNA Detection with a Water-Gated Organic Field-Effect Transistor. *Org. Electron.* **2012**, *13*, 1–6.

(24) Buth, F.; Kumar, D.; Stutzmann, M.; Garrido, J. a. Electrolyte-Gated Organic Field-Effect Transistors for Sensing Applications. *Appl. Phys. Lett.* **2011**, *98*, 153302.

(25) Buth, F.; Donner, A.; Sachsenhauser, M.; Stutzmann, M.; Garrido, J. a. Biofunctional Electrolyte-Gated Organic Field-Effect Transistors. *Adv. Mater.* **2012**, *24*, 4511–4517.

(26) Magliulo, M.; Mallardi, A.; Mulla, M. Y.; Cotrone, S.; Pistillo, B. R.; Favia, P.; Vikholm-Lundin, I.; Palazzo, G.; Torsi, L. Electrolyte-Gated Organic Field-Effect Transistor Sensors Based on Supported Biotinylated Phospholipid Bilayer. *Adv. Mater.* **2012**, 1–5.

(27) Evans, E.; Ritchie, K. Dynamic Strength of Molecular Adhesion Bonds. *Biophys. J.* **1997**, *72*, 1541–1555.

(28) Merkel, R.; Nassoy, P.; Leung, A.; Ritchie, K.; Evans, E. Energy Landscapes of Receptor-Ligand Bonds Explored with Dynamic Force Spectroscopy. *Nature* **1999**, *397*, 50–53.

(29) Medalsy, I. D.; Müller, D. J. Nanomechanical Properties of Proteins and Membranes Depend on Loading Rate and Electrostatic Interactions. *ACS Nano* **2013**, *7*, 2642–2650.

(30) Florin, E. L.; Moy, V. T.; Gaub, H. E. Adhesion Forces between Individual Ligand-Receptor Pairs. *Science (80-.).* **1994**, *264*, 415–417.

(31) Moy, V. T.; Florin, E. L.; Gaub, H. E. Intermolecular Forces and Energies between Ligands and Receptors. *Science* **1994**, *266*, 257–259.

(32) Hinterdorfer, P.; Baumgartner, W.; Gruber, H. J.; Schilcher, K.; Schindler, H. Detection and Localization of Individual Antibody-Antigen Recognition Events by Atomic Force Microscopy. *Proc. Natl. Acad. Sci.* **1996**, *93*, 3477–3481.

(33) Brogan, K. L.; Schoenfisch, M. H. Influence of Antibody Immobilization Strategy on Molecular Recognition Force Microscopy Measurements. *Langmuir* **2005**, *21*, 3054–3060.

(34) Carrion-Vazquez, M.; Oberhauser, A. F.; Fowler, S. B.; Marszalek, P. E.; Broedel, S. E.; Clarke, J.; Fernandez, J. M. Mechanical and Chemical Unfolding of a Single Protein: A Comparison. *Proc. Natl. Acad. Sci.* **1999**, *96*, 3694–3699.

(35) Rief, M.; Gautel, M.; Oesterhelt, F.; Fernandez, J. M.; Gaub, H. E. Reversible Unfolding of Individual Titin Immunoglobulin Domains by AFM. *Science (80-.).* **1997**, *276*, 1109–1112.

(36) Tromas, C.; Rojo, J.; de la Fuente, J. M.; Barrientos, A. G.; García, R.; Penadés, S. Adhesion Forces between LewisX Determinant Antigens as Measured by Atomic Force Microscopy. *Angew. Chemie Int. Ed.* **2001**, *40*, 3052–3055.

(37) Müller, D. J.; Dufrêne, Y. F. Force Nanoscopy of Living Cells. *Curr. Biol.* **2011**, *21*, R212–R216.

(38) Ledeboer, A.; Brevé, J. J. P.; Poole, S.; Tilders, F. J. H.; Dam, A. V. A. N. Interleukin-10, Interleukin-4 and Transforming Growth Factor-Beta Differentially Regulate Lipopolysaccharide-Induced Production of pro-Inflammatory Cytokines and Nitric Oxide in Co-Cultures of Rat Astroglial and Microglial Cells. *Glia* **2000**, *30*, 134–142.

(39) Wirjatijasa, F.; Dehghani, F.; Blaheta, R. a; Korf, H.-W.; Hailer, N. P. Interleukin-4, Interleukin-10, and Interleukin-1-Receptor Antagonist but Not Transforming Growth Factor-Beta Induce Ramification and Reduce Adhesion Molecule Expression of Rat Microglial Cells. *J. Neurosci. Res.* **2002**, *68*, 579–587.

(40) Yang, M.-S.; Park, E. J.; Sohn, S.; Kwon, H. J.; Shin, W.-H.; Pyo, H. K.; Jin, B.; Choi, K. S.; Jou, I.; Joe, E.-H. Interleukin-13 and -4 Induce Death of Activated Microglia. *Glia* **2002**, *38*, 273–280.

(41) Lee, S. I.; Jeong, S. R.; Kang, Y. M.; Han, D. H.; Jin, B. K.; Namgung, U.; Kim, B. G. Endogenous Expression of Interleukin-4 Regulates Macrophage Activation and Confines Cavity Formation after Traumatic Spinal Cord Injury. *J. Neurosci. Res.* **2010**, *88*, 2409–2419.

(42) Betancor, L.; López-Gallego, F.; Hidalgo, A.; Alonso-Morales, N.; Mateo, G. D.-O. C.; Fernández-Lafuente, R.; Guisán, J. M. Different Mechanisms of Protein Immobilization on Glutaraldehyde Activated Supports: Effect of Support Activation and Immobilization Conditions. *Enzyme Microb. Technol.* **2006**, *39*, 877–882.

(43) Walt, D. R.; Agayn, V. I. The Chemistry of Enzyme and Protein Immobilization with Glutaraldehyde. *Trends Anal. Chem.* **1994**, *13*, 425–430.

(44) Yang, Z.; Zhao, Y.-P. Adsorption of His-Tagged Peptide to Ni, Cu and Au (100) Surfaces: Molecular Dynamics Simulation. *Eng. Anal. Bound. Elem.* **2007**, *31*, 402–409.

(45) Soong, R. K.; Stelick, S. J.; Bachand, G. D.; Montemagno, C. D. Evaluating Adhesion Strength of Biological Molecules to Nanofabricated Substrates. In *INTERNATIONAL CONFERENCE ON MODELING AND SIMULATION OF MICROSYSTEMS*; 1999; pp. 95–98.

(46) Bachand, G. D.; Montemagno, C. D. Constructing Organic / Inorganic NEMS Devices Powered by Biomolecular Motors. *Biomed. Microdevices* **2000**, *2:3*, 179–184.

(47) Baio, J. E.; Cheng, F.; Ratner, D. M.; Stayton, P. S.; Castner, D. G. Probing Orientation of Immobilized Humanized Anti-Lysozyme Variable Fragment by Time-of-Flight Secondary-Ion Mass Spectrometry. *J. Biomed. Mater. Res. A* **2011**, 1–7.

(48) Trilling, A. K.; Beekwilder, J.; Zuilhof, H. Antibody Orientation on Biosensor Surfaces: A Minireview. *Analyst* **2013**, *138*, 1619–1627.

(49) Bae, Y. M.; Oh, B.-K.; Lee, W.; Lee, W. H.; Choi, J.-W. Study on Orientation of Immunoglobulin G on Protein G Layer. *Biosens. Bioelectron.* **2005**, *21*, 103–110.

(50) Song, H. Y.; Zhou, X.; Hobley, J.; Su, X. Comparative Study of Random and Oriented Antibody Immobilization as Measured by Dual Polarization Interferometry and Surface Plasmon Resonance Spectroscopy. *Langmuir* **2012**, *28*, 997–1004.

(51) Mark, L. W.; Smith, D. A. Complex Chemical Force Titration Behavior of Amine-Terminated Self-Assembled Monolayers. *Langmuir* **2001**, *17*, 1126–1131.

(52) San Paulo, A.; García, R. Attractive and Repulsive Tip-Sample Interaction Regimes in Tapping-Mode Atomic Force Microscopy. *Phys. Rev. B* **1999**, *60*, 4961–4967.

(53) Zhao, X.; Yaseen, M.; Pan, F.; Lu, J. R.; Street, M.; Sheffield, S. *Protein and Interfaces III. State of the Art*; 2012; pp. 543–574.

(54) Ido, S.; Kimiya, H.; Kobayashi, K.; Kominami, H.; Matsushige, K.; Yamada, H. Immunoactive Two-Dimensional Self-Assembly of Monoclonal Antibodies in Aqueous Solution Revealed by Atomic Force Microscopy. *Nat. Mater.* **2014**, *13*, 264–270.

(55) Press, W. H.; Teukolsky, S. A.; Vetterling, W. T.; Flannery, B. P. *Numerical Recipes, The Art of Scientific Computing*; 2007.

(56) Abramowitz, M.; Stegun, I. A. *Handbook of Mathematical Functions with Formulas, Graphs, and Mathematical Tables*; 1972.

(57) Biscarini, F.; Zamboni, R.; Samorì, P.; Ostoja, P.; Taliani, C. Growth of Conjugated Oligomer Thin Films Studied by Atomic-Force Microscopy. *Phys. Rev. B* **1995**, *52*, 14868–14877.

(58) Schwesinger, F.; Ros, R.; Strunz, T.; Anselmetti, D.; Güntherodt, H.-J.; Honegger, A.; Jermutus, L.; Tiefenauer, L.; Plückthun, A. Unbinding Forces of Single Antibody-Antigen Complexes Correlate with Their Thermal Dissociation Rates. *Proc. Natl. Acad. Sci.* **2000**, *97*, 9972–9977.

(59) Brogan, K. L.; Shin, J. H.; Schoenfisch, M. H. Influence of Surfactants and Antibody Immobilization Strategy on Reducing Nonspecific Protein Interactions for Molecular Recognition Force Microscopy. *Langmuir* **2004**, *20*, 9729–9735.

(60) Berquand, A.; Xia, N.; Castner, D. G.; Clare, B. H.; Abbott, N. L.; Dupres, V.; Adriaensen, Y.; Dufrene, Y. F. Antigen Binding Forces of Single Antilysozyme Fv Fragments Explored by Atomic Force Microscopy. *Langmuir* **2005**, *21*, 5517–5523.

(61) Kienberger, F.; Kada, G.; Mueller, H.; Hinterdorfer, P. Single Molecule Studies of Antibody-Antigen Interaction Strength versus Intra-Molecular Antigen Stability. *J Mol Biol* **2005**, *347*, 597–606.

(62) Van Es, M. H.; Tang, J.; Preiner, J.; Hinterdorfer, P.; Oosterkamp, T. H. Single Molecule Binding Dynamics Measured with Atomic Force Microscopy. *Ultramicroscopy* **2014**, *140*, 32–36.

(63) Bizzarri, A. R.; Cannistraro, S. The Application of Atomic Force Spectroscopy to the Study of Biological Complexes Undergoing a Biorecognition Process. *Chem Soc Rev* **2010**, *39*, 734–749.

(64) Bonanni, B.; Bizzarri, A. R.; Cannistraro, S. Optimized Biorecognition of Cytochrome c 551 and Azurin Immobilized on Thiol-Terminated Monolayers Assembled on Au (111) Substrates. *J. Phys. Chem. B* **2006**, *551*, 14574–14580.

(65) Bonanni, B.; Kamruzzahan, A. S. M.; Bizzarri, A. R.; Rankl, C.; Gruber, H. J.; Hinterdorfer, P. Single Molecule Recognition between Cytochrome C 551 and Gold-Immobilized Azurin by Force Spectroscopy. *Biophys. J.* **2005**, *89*, 2783–2791.

(66) Eyring, H. The Activated Complex in Chemical Reactions. *J. Chem. Phys.* **1935**, *3*, 107–115.

(67) Oesterhelt, F.; Rief, M.; Gaub, H. E. Single Molecule Force Spectroscopy by AFM Indicates Helical Structure of Poly (Ethylene-Glycol) in Water. *New J. Phys.* **1999**, *1*, 6.1–6.11.

(68) Walczak, M.; Popenoe, D. D.; Deinhammer, R. S.; Lamp, B. D.; Chung, C.; Porter, M. D. Reductive Desorption of Alkanethiolate Monolayers at Gold: A Measure of Surface Coverage. *Langmuir* **1991**, 2687–2693.

(69) Widrig, A.; Porter, M. D. The Electrochemical Desorption of N-Alkanethiol from Polycrystalline Au and Ag Electrodes Monolayers. *J. Electroanal. Chem.* **1991**, *310*, 335–359.

(70) Campana, A.; Cramer, T.; Greco, P.; Foschi, G.; Murgia, M.; Biscarini, F. Facile Maskless Fabrication of Organic Field Effect Transistors on Biodegradable Substrates. *Appl. Phys. Lett.* **2013**, *103*, 073302.

(71) Casalini, S.; Shehu, A.; Destri, S.; Porzio, W.; Pasini, M. C.; Vignali, F.; Borgatti, F.; Albonetti, C.; Leonardi, F.; Biscarini, F. Organic Field-Effect Transistors as New Paradigm for Large-Area Molecular Junctions. *Org. Electron.* **2012**, *13*, 789–795.

(72) Garcıa, R.; San Paulo, A. Attractive and Repulsive Tip-Sample Interaction Regimes in Tapping-Mode Atomic Force Microscopy. *Phys. Rev. B* **1999**, *60*, 4961–4967.

(73) Herruzo, E. T.; Garcia, R. Frequency Response of an Atomic Force Microscope in Liquids and Air: Magnetic versus Acoustic Excitation. *Appl. Phys. Lett.* **2007**, *91*, 143113.

(74) Butt, H.-J.; Jaschke, M. Calculation of Thermal Noise in Atomic Force Microscopy. *Nanotechnology* **1995**, *6*, 1–7.

SUPPORTING INFO

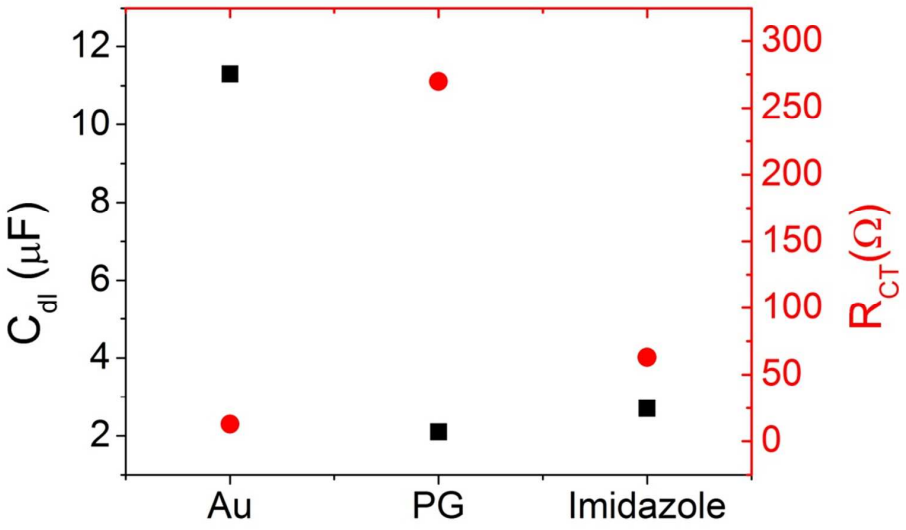

Figure S1 Overlay of the double-layer capacitance and charge transfer resistance for bare Au, PG adsorbed on it and imidazole elution.

Electrode modifiers	C_{dl} (µF)	R_{CT} (kΩ)
HSC_6NH_2	1.3(±0.1)	0.7(±0.1)
HSC_6NH_2 + Anti-IL4	0.56(±0.07)	2.3 (±0.1)
PG	1.14(±0.02)	3.1(±0.1)
PG + Anti-IL4	1.22(±0.02)	4.3(±0.1)

Table S1 C_{dl} and R_{CT} values are listed for the two functionalization protocols.

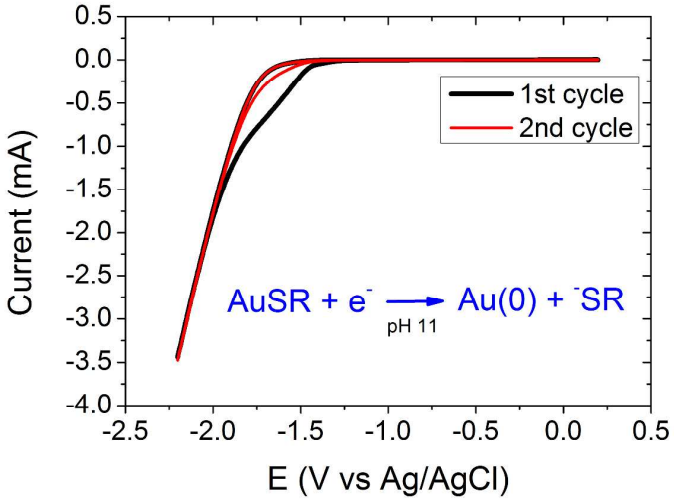

Figure S2 Reductive electrochemical desorption of the bio-material chemically adsorbed on polycrystalline Au. First scan (black line) and second one (red line) are overlayed.

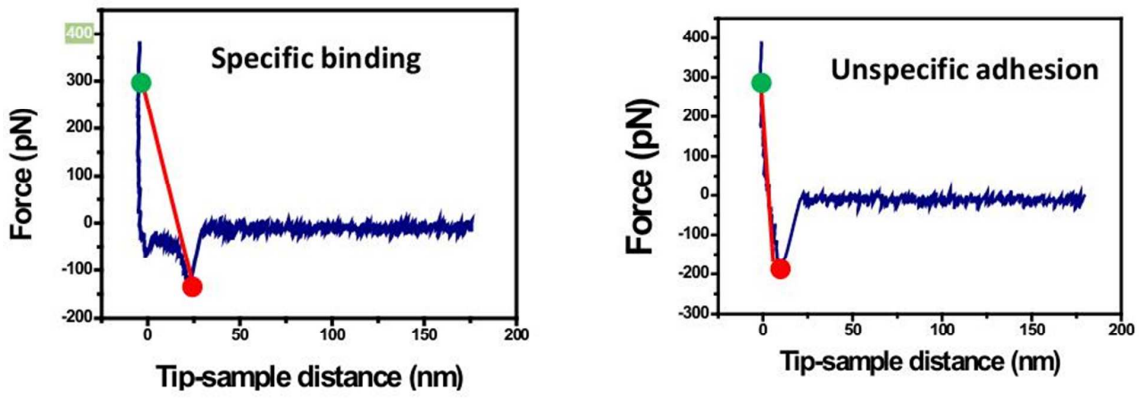

Figure S4 Scheme of the algorithm used to discriminate between specific recognition event, and unspecific adhesion.

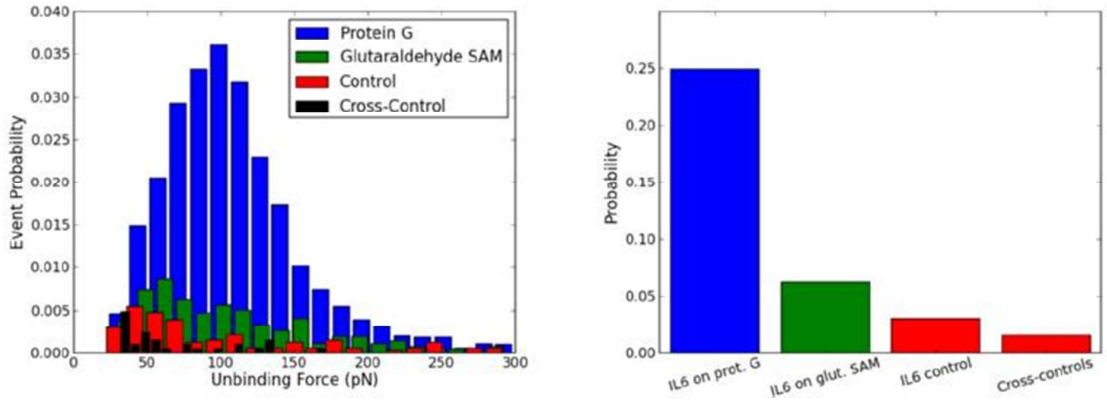

Figure S5 (a) Histogram and (b) bar-plot of the probability percentage for specific, aspecific immobilization, control experiments for IL6 antibody-antigen recognition.

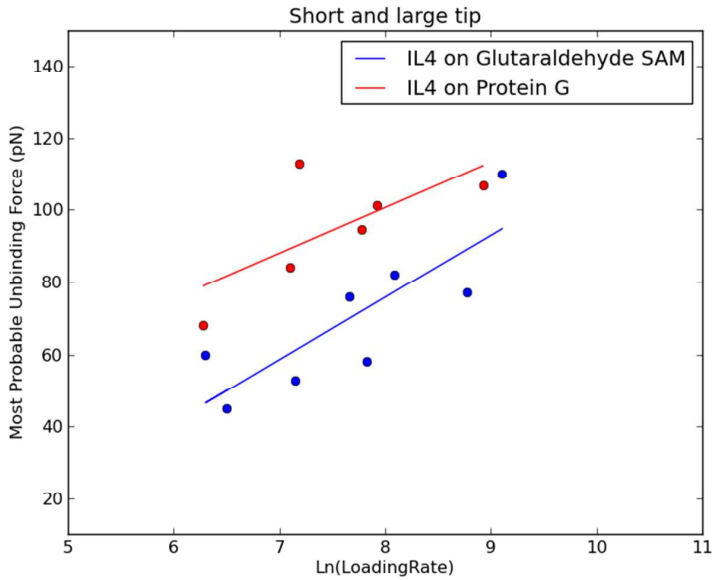

Figure S6 Most probable unbinding force vs loading rate for (a) aspecific and (b) specific functionalization: